PERGAMON

Chemical Engineering Science 54 (1999) 3305–3314

Chemical Engineering Science

Plasma enhanced chemical vapor deposition: Modeling and control

Antonios Armaou, Panagiotis D. Christofides*

Department of Chemical Engineering, University of California, Los Angeles, CA 90095-1592, USA

Abstract

This paper focuses on modeling and control of a single-wafer parallel electrode plasma-enhanced chemical vapor deposition process with showerhead arrangement used to deposit a 500 Å amorphous silicon thin film on an 8 cm wafer. Initially, a two-dimensional unsteady-state model is developed for the process that accounts for diffusive and convective mass transfer, bulk and deposition reactions, and nonuniform fluid flow and plasma electron density profiles. The model is solved using finite-difference techniques and the radial nonuniformity of the final film thickness is computed to be almost 19%. Then, a feedback control system is designed and implemented on the process to reduce the film thickness nonuniformity. The control system consists of three spatially distributed proportional integral controllers that use measurements of the deposition rate at several locations across the wafer, to manipulate the inlet concentration of silane in the showerhead and achieve a uniform deposition rate across the wafer. The implementation of the proposed control system is shown to reduce the film thickness radial nonuniformity to 3.8%. © 1999 Elsevier Science Ltd. All rights reserved.

Keywords: Plasma processes; Amorphous silicon deposition; Distributed control action; Proportional-integral control

1. Introduction

Single-wafer plasma-enhanced chemical vapor deposition (PECVD) is an emerging technology used in microelectronics industry to deposit thin films of compounds (e.g. amorphous silicon, silicon nitride, etc.) on substrates. In a PECVD process, the activation of the reacting gases is achieved through impact with electrons. This is in contrast to conventional chemical vapor deposition where the reacting gases are activated thermally. The main advantage of plasma assisted activation of the reacting gases is that low operational temperatures (compared to the ones required in conventional chemical vapor deposition processes) are achieved, thereby allowing the deposition of high-temperature sensitive films. An additional advantage of PECVD processes is the relatively high deposition rate which results in a significant reduction in the processing time; a very important benefit for single wafer processing. The ability to treat devices that are sensitive to heating and the high deposition rate make PECVD an attractive alternative over conventional furnace-based chemical vapor deposition processes employed in the fabrication of devices with submicron dimensional constraints. However, at this stage, the widespread use of PECVD is seriously limited by the significant spatial nonuniformity of the deposition rate which, in many cases, violates the tight requirements set by the industry.

The design and operation of PECVD processes that achieve the desired performance specifications requires the derivation of accurate mathematical models that can be used to design optimal reactor and flow arrangements and test the performance of different control systems. The key issue in the development of high-fidelity models for PECVD processes is the understanding and characterization of the physico-chemical phenomena taking place in such processes including glow discharge chemistry, electron density and energy distribution, ion transport, diffusive and convective mass transfer, bulk and deposition reaction kinetics. Fortunately, significant research has been carried out in this direction including the characterization of plasma chemistry (e.g., Kushner, 1988;

*Corresponding author. Tel.: 001 310 794 1015; fax: 001 310 206 4107; e-mail- pdc@scas.ucla.edu.

0009-2509/99/$ – see front matter © 1999 Elsevier Science Ltd. All rights reserved.
PII: S0009-2509(98)00458-8

Austin and Lampe, 1976; Doyle et al., 1990), the experimental measurement of electron density profiles in plasma reactors (e.g., Belenguer and Boeuf, 1990; Bohm and Perrin, 1991), and the identification of bulk and deposition reactions and their mechanisms (e.g., Perrin and Broekhuizen, 1987; Gallagher, 1988; Perrin et al., 1989; Doughty et al., 1990).

The improved understanding of plasma physics and chemistry has led to the development of fundamental mathematical models for various plasma-assisted etching and deposition processes. In this area, important contributions include the development of comprehensive models for plasma etching processes (Economou et al., 1989; Park and Economou, 1990; Park and Economou, 1991), and more recently, for PECVD reactors used to deposit silicon nitride thin films (Layeillon et al., 1994a; Layeillon et al., 1995; Caquineau and Despax, 1997). These models were used in the design of reactor configurations that reduce the radial etching rate and deposition rate nonuniformity. For example, it was established that the use of a showerhead arrangement instead of the conventional single opening one, to enter the precursor gas into the reaction chamber, reduces significantly the radial etching and film thickness nonuniformity. Despite the recent advances on modeling of PECVD processes, there are still many PECVD processes for which detailed mathematical models are not available including the one used to deposit amorphous silicon thin films. Furthermore, available results on control of plasma-assisted processes are mainly limited to plasma etching (e.g., McLaughlin et al., 1991a; McLaughlin et al., 1991b; Mozumder et al., 1994), thereby motivating further the study of modeling and control of PECVD processes.

In this work, we consider a single-wafer parallel electrode PECVD process with showerhead arrangement used to deposit a 500 Å amorphous silicon thin film on an 8 cm wafer. The objective is to develop a detailed fundamental model for this process, able to predict the deposition rate profile across the radius of the wafer, and a feedback control strategy that can substantially reduce deposition rate radial nonuniformity. Initially, a two-dimensional unsteady-state model is developed that accounts for diffusive and convective mass transfer, bulk and deposition reactions, and nonuniform fluid flow and plasmaelectron density profiles. The model predicts that the radial film thickness nonuniformity is almost 19%. Then, a feedback control system is designed and implemented on the process to reduce the film thickness nonuniformity. The control system consists of three spatially distributed proportional integral controllers that use measurements of the deposition rate at several locations across the wafer, to manipulate the inlet concentration of silane in the showerhead and achieve a uniform deposition rate across the wafer. The implementation of the proposed control system is shown to reduce the film thickness nonuniformity to 3.8%. The robustness propertiesof the control system with respect to disturbances are also tested.

2. Process description and modeling

We consider a single-wafer parallel electrode PECVD process with showerhead arrangement shown in Fig. 1. The objective of the process is to deposit a 500 Å amorphous silicon thin film on an 8 cm wafer, which is placed on the top of the lower electrode. The reactor is fed through the showerhead by a gas stream consisting of silane, SiH_4, and inert gases (typically H_2 or He). The flow rate and composition of the influent gas stream is assumed to be uniform throughout the showerhead. An RF (radio frequency) power source is used to generate the plasma (i.e. chemically reactive mixture of ions, electrons and radicals) from silane. The radicals are then transported via convection and diffusion to the surface of the wafer where they react and deposit amorphous silicon. Plasma species that do not deposit and unreacted silane are pumped radially outwards. The reactor is assumed to be at 1 Torr pressure and 500 K temperature, while a 13.56 MHz frequency alternate voltage is applied to the electrodes generating a glow discharge. In the remainder of this section, we develop a fundamental model for the PECVD reactor of Fig. 1.

2.1. Flow field

The gas flow inside the PECVD reactor of Fig. 1 resembles the three-dimensional axisymmetric stagnation flow. Under the standard assumptions: (a) treating plasma as a continuum medium, (b) constant physical properties of the gas, (c) negligible volume change of the reacting gases, and (d) azimuthal reactor symmetry, the evolution of the velocity profile inside the PECVD reactor can be computed from the Navier-Stokes and continuity equations

$$\frac{\partial v_r}{\partial t} + v_r \frac{\partial v_r}{\partial r} + v_z \frac{\partial v_r}{\partial z} = -\frac{1}{\rho}\frac{\partial P}{\partial r} + \nu\left(\frac{\partial^2 v_r}{\partial r^2} + \frac{1}{r}\frac{\partial v_r}{\partial r} - \frac{v_r}{r^2} + \frac{\partial^2 v_r}{\partial z^2}\right),$$

$$\frac{\partial v_z}{\partial t} + v_r \frac{\partial v_z}{\partial r} + v_z \frac{\partial v_z}{\partial z} = -\frac{1}{\rho}\frac{\partial P}{\partial z} + \nu\left(\frac{\partial^2 v_z}{\partial r^2} + \frac{1}{r}\frac{\partial v_z}{\partial r} + \frac{\partial^2 v_z}{\partial z^2}\right), \quad (1)$$

$$\frac{\partial v_r}{\partial r} + \frac{v_r}{r} + \frac{\partial v_z}{\partial z} = 0,$$

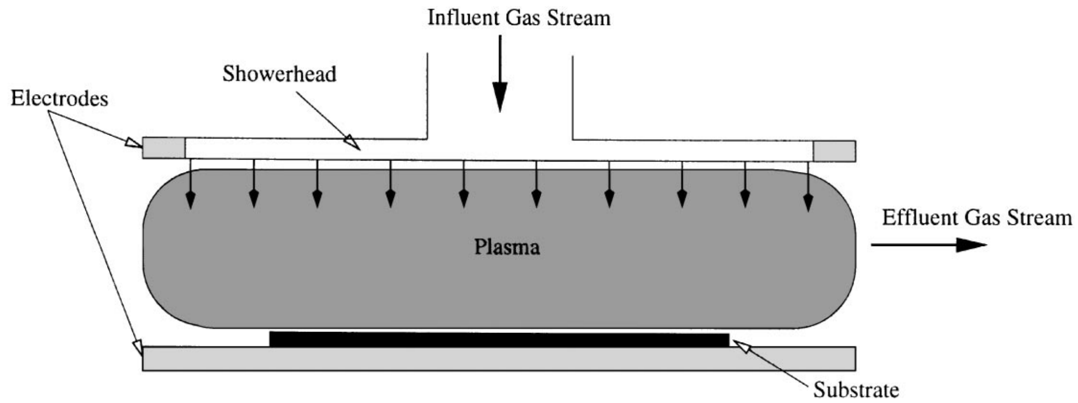

Fig. 1. Cylindrical showerhead electrode plasma enhanced CVD reactor.

subject to the boundary conditions

$$v_r(r, 0) = 0, \quad v_z(r, 0) = 0,$$

$$v_r(r, L) = 0, \quad v_z(r, L) = -v_w \tag{2}$$

where v_r is the velocity in the r-direction, v_z is the velocity in the z-direction, $r \in [0, r_t]$ is the radial coordinate, r_t is the radius of the reactor, $z \in [0, L]$ is the axial coordinate, L is the height of the reactor (i.e. distance between the two electrodes), ρ is the (constant) density of the plasma, P is the pressure, ν is the (constant) kinematic viscosity defined as $\nu = \mu/\rho$, μ is the (constant) viscosity of the plasma, and v_w is the velocity of the feed gas entering the chamber. The velocity of the feed gas at the upper electrode is assumed to be uniform and is calculated from the equation: $v_w = Q(T, P)/N_h \pi r_h^2$, where $Q(T, P)$ is the volumetric rate of the precursor gas at the operating conditions of the reactor, N_h is the number of holes on the top electrode, and r_h is the radius of each hole.

Defining the wall Reynolds number as $Re_w = v_w L/4\nu$, using that for the reactor of Fig. 1, $Re_w = 0.49 < 1$ (the computation of Re_w was made by using the values of Table 1) and assuming that v_z is only a function of z, the following steady-state approximate analytic solution of the Navier–Stokes and continuity equations of Eq. (1) can be computed (see also Economou et al. (1989)):

$$v_r(z, r) = \frac{v_w}{L} r \left[-\frac{3}{4}\psi^2 + \frac{3}{4} + Re_w \left(-\frac{1}{160}\psi^6 + \frac{3}{32}\psi^4 + \frac{1}{4}\psi^3 - \frac{117}{1120}\psi^2 - \frac{1}{4}\psi + \frac{19}{1120} \right) \right],$$

$$y_z(z) = -v_w \left[-\frac{1}{4}\psi^3 + \frac{3}{4}\psi + \frac{1}{2} + Re_w \left(-\frac{1}{1120}\psi^7 + \frac{3}{160}\psi^5 + \frac{1}{16}\psi^4 - \frac{39}{1120}\psi^3 - \frac{1}{8}\psi^2 + \frac{19}{1120}\psi + \frac{1}{16} \right) \right],$$

Table 1
Process parameters

$P = 1.0$	Torr
$T = 500$	K
$L = 3.6$	cm
$r_t = 8.0$	cm
$r_w = 4.0$	cm
$Q = 50.0$	s cm^3 min^{-1}
$N_h = 350$	
$r_h = 0.1$	cm
$n_{eo} = 2.0 \times 10^{10}$	cm^{-3}
$\mu = 1.832 \times 10^{-7}$	kg s^{-1} cm^{-1}
$\rho = 1.030 \times 10^{-9}$	kg cm^{-3}
$\rho_{Si} = 8.292 \times 10^{-10}$	mol A^{-1} cm^{-2}

where $\psi = 2z/L - 1$. The above analytic expressions for $v_r(z, r)$ and $v_z(z)$ were employed in the simulations of Sections 3 and 4.

2.2. Electron density profile

For 1 Torr pressure and 13.56 MHz frequency alternate voltage, the secondary electron emission is negligible and the glow is mainly sustained by bulk ionization. Therefore, the steady-state electron density profile is computed by assuming diffusion-controlled discharge in a cylindrical container and is given by the following formula (Park and Economou, 1991):

$$n_e(r, z) = n_{eo} J_0 \left(2.405 \frac{r}{r_t} \right) \sin\left(\frac{\pi z}{L} \right) \tag{4}$$

where $n_e(r, z)$ is the electron density, n_{eo} is the maximum electron density in the reactor (n_{eo} depends on the power dissipated in the plasma, the plasma volume and the effective electric field; the value of n_{eo} used in our calculations was computed in Bohm and Perrin (1991) from experimental data), J_0 is the zero order Bessel function of the first kind and r_t is the radius of the reactor. From Eq. (4), it is clear that the electron density profile attains

its maximum value in the center of the reactor (i.e. $r = 0$, $z = L/2$).

2.3. Reactions and mass transport

Regarding the reactions that take place on the bulk of the plasma, we assume that SiH_4 enters the reactor and dissociates according to the following reaction scheme:

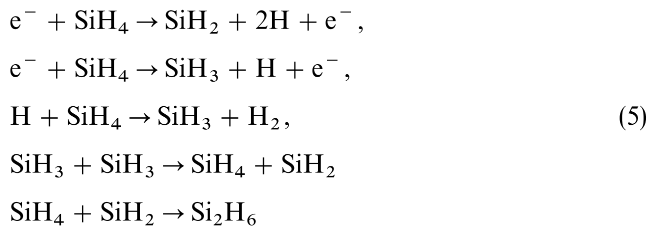

$$\begin{aligned} &e^- + SiH_4 \rightarrow SiH_2 + 2H + e^-, \\ &e^- + SiH_4 \rightarrow SiH_3 + H + e^-, \\ &H + SiH_4 \rightarrow SiH_3 + H_2, \\ &SiH_3 + SiH_3 \rightarrow SiH_4 + SiH_2 \\ &SiH_4 + SiH_2 \rightarrow Si_2H_6 \end{aligned} \tag{5}$$

where e^- is the electron, SiH_2 is the silylene radical, SiH_3 is the silyl radical, Si_2H_6 is the disilane and H is the atomic hydrogen. The reaction scheme of Eq. (5) was proposed in Hamby et al. (1994) and Layeillon et al. (1994b) to represent various sets of experimental data. According to this reaction scheme, SiH_4 initially dissociates due to electron impact forming silylene, silyl radicals and atomic hydrogen; this stage is described by the following reactions:

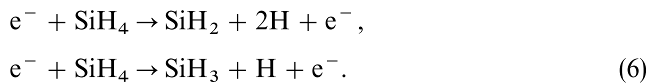

$$\begin{aligned} &e^- + SiH_4 \rightarrow SiH_2 + 2H + e^-, \\ &e^- + SiH_4 \rightarrow SiH_3 + H + e^-. \end{aligned} \tag{6}$$

The hydrogen radical H then reacts with SiH_4 according to the following abstraction reaction forming SiH_3:

$$H + SiH_4 \rightarrow SiH_3 + H_2 \cdot \tag{7}$$

SiH_3 diffuses towards the surface of the wafer where the following recombination reaction occurs:

$$SiH_3 + SiH_3 \rightarrow SiH_4 + SiH_2 \cdot \tag{8}$$

The following insertion reaction forming disilane also takes place:

$$SiH_4 + SiH_2 \rightarrow Si_2H_6. \tag{9}$$

Assuming that the effective reaction rates of the reactions of Eq. (5) can be expressed as a product of the dissociation constants, electron density and reactant species concentrations (Kushner, 1988), the following expressions can be written for the rate of change of the concentration, $r_{x,i}$, of the species SiH_4, SiH_2, SiH_3, H due to consumption and production according to the reactions of Eq. (5):

$$\begin{aligned} r_{x,1} &= -k_1 n_e c_1 - k_2 n_e c_1 - k_3 c_1 c_4 + k_4 c_3 c_3 - k_5 c_1 c_2, \\ r_{x,2} &= k_1 n_e c_1 + k_4 c_3 c_3 - k_5 c_1 c_2, \\ r_{x,3} &= k_2 n_e c_1 + k_3 c_1 c_4 - 2k_4 c_3 c_3, \\ r_{x,4} &= 2k_1 n_e c_1 + k_2 n_e c_1 - k_3 c_1 c_4 \end{aligned} \tag{10}$$

where the subscripts $i = 1, 2, 3, 4$ correspond to silane SiH_4, silylene radical SiH_2, silyl radical SiH_3, and atomic hydrogen H, respectively, c_i is the concentration of each species, and k_j, $j = 1, 2, 3, 4, 5$, is the reaction rate constant for each reaction in the scheme of Eq. (5).

Owing to the complex and poorly understood nature of the deposition reactions, we assume that SiH_3 and SiH_2 approach the wafer surface and instantaneously react towards SiH_4 and a-Si, and a-Si and H_2, respectively. To determine the amount of SiH_4 and a-Si being produced by the deposition reactions, we use the concepts of sticking and recombination probabilities (see also Perrin et al., 1989; Doyle et al., 1990; Austin and Lampe, 1976). Specifically, we compute the amount of a-Si and SiH_4 produced by the deposition reactions of SiH_3 by multiplying the flux of SiH_3 on the wafer surface by s_3 (sticking probability) and γ_3 (recombination probability), respectively. The amount of a-Si which is produced by the deposition reactions of SiH_2 is computed by multiplying the flux of SiH_2 on the wafer surface by s_2 (sticking probability). We note that the contribution of disilane Si_2H_6 in a-Si deposition at 500 K is negligible (Layeillon et al., 1994), and thus, it is not included in our calculations.

Applying dynamic material balances to the process and accounting for diffusive and convective mass transfer, and bulk and surface reactions, a mathematical model that describes the spatio-temporal evolution of the concentration of the species, SiH_4, SiH_2, SiH_3 and H, throughout the reactor is obtained. The model consists of four nonlinear parabolic partial differential equations and can be written in the following compact form:

$$\begin{aligned} \frac{\partial c_i}{\partial t} &= D_i\left(\frac{\partial^2 c_i}{\partial r^2} + \frac{1}{r}\frac{\partial c_i}{\partial r} + \frac{\partial^2 c_i}{\partial x^2}\right) - v_r \frac{\partial c_i}{\partial r} - v_z \frac{\partial c_i}{\partial z} \\ &\quad + r_{x,i}(n_e, c_1, c_2, c_3, c_4), \quad i = 1, \ldots, 4 \end{aligned} \tag{11}$$

subject to the boundary conditions:

$$\frac{\partial c_i}{\partial r}(t, 0, z) = 0, \quad \frac{\partial c_i}{\partial r}(t, r_t, z) = 0, \quad i = 1, \ldots, 4, \tag{12}$$

$$c_i(t, r, L) = c_{w,i}(t, r), \quad i = 1, \ldots, 4, \tag{13}$$

$$\begin{aligned} &\frac{\partial c_1}{\partial z}(t, r, 0) = -\gamma_3 \frac{D_3}{D_1}\frac{\partial c_3}{\partial z}(t, r, 0), \quad c_2(t, r, 0) = 0, \\ &c_3(t, r, 0) = 0; \quad \frac{\partial c_4}{\partial z}(t, r, 0) = 0, \quad 0 \leqslant r \leqslant r_w, \end{aligned} \tag{14}$$

$$\frac{\partial c_i}{\partial z}(t, r, 0) = 0, \quad i = 1, \ldots, 4, \quad r_w < r \leqslant r_t \tag{15}$$

and the initial conditions:

$$c(0, r, z) = c_i^0(r, z), \quad i = 1, \ldots, 4 \tag{16}$$

where D_i is the diffusion coefficient of the ith species, r_w is the radius of the wafer, $c_{w,i}(t)$ is the concentration of the specific species at the feed, $c_i^0(r, z)$ is the concentration of the species initially in the chamber, and γ_3 represents the

percentage of SiH_3 surface reaction leading to SiH_4 (recombination probability). The boundary condition

$$\frac{\partial c_1}{\partial z}(t,r,0) = -\gamma_3 \frac{D_3}{D_1}\frac{\partial c_3}{\partial z}(t,r,0)$$

accounts for the production of SiH_4 by SiH_3 consumption on the wafer surface, the boundary conditions $c_2(t,r,0) = 0$, $c_3(t,r,0) = 0$ express the instantaneous consumption of SiH_2 and SiH_3 on the wafer surface, and the boundary condition

$$\frac{\partial c_4}{\partial z}(t,r,0) = 0$$

accounts for nonflux of H on the wafer. The boundary conditions outside of the wafer surface (Eq. (15)) result from the fact that SiH_4, SiH_2, SiH_3, H do not react with the walls of the reactor. The deposition rate of amorphous silicon on the wafer is calculated from the following equation:

$$R_{\mathrm{dep}}(t,r) = \frac{1}{\rho_{Si}}\left[\sum_{i=1}^{4} s_i D_i \frac{\partial c_i}{\partial z}(t,r,0)\right], \tag{17}$$

where ρ_{Si} is the density of $a-Si$ and s_i represents the percentage of the flux of the ith species towards the surface leading to deposition of amorphous silicon (sticking probability).

The values of the operating conditions and the reactor parameters are given in Table 1, the values of the reaction rate constants are presented in Table 2, and finally, the values of physico-chemical properties of the species are tabulated in Table 3. We note that: (a) the physical properties of the plasma (e.g. viscosity) were computed by assuming that the plasma consists of pure silane, (b) the density of the mixture was calculated from the ideal gas law, and (c) the diffusion coefficients of the radicals and the silane were calculated from equations based on Lennard–Jones potential under the assumption that all the species diffuse through pure silane (see also Reid et al., 1987; Hirschfelder et al., 1954).

3. Open-loop simulation results

The mathematical model of the PECVD reactor of Fig. 1 consisting of the four unsteady-state two-dimensional diffusion-reaction equations (Eq. (11)), the velocity (Eq. (3)) and electron density (Eq. (4)) profiles, was solved using numerical techniques. Specifically, the finite-difference method was initially used to discretize the spatial derivatives of Eq. (11) in the r and z directions (75 and 75 discretization points were used in the r and z direction, respectively; it was verified that further increase in the number of discretization points in both r and z directions results in insignificant improvements in the accuracy of the computed solution). Then, the time integration of the resulting large (75×75) set of ordinary differential equations was performed by utilizing the alternate direction implicit (ADI) method. In all the simulation runs, the reactor is initially assumed to be filled with pure silane.

Fig. 2 shows the profile of the steady-state dimensionless concentration of silane, SiH_4, inside the reactor (in the r-axis: 0 cm is the center of the wafer, 4.0 cm is the edge of the wafer and 8.0 cm is the edge of the reactor; in the z-axis: 0 cm is the wafer surface and 3.6 cm is the showerhead). We observe that the concentration of silane is lower towards the center of the reactor. This is because silane is mainly consumed by the dissociation reactions, $e^- + SiH_4 \rightarrow SiH_2 + 2H$, $e^- + SiH_4 \rightarrow SiH_3 + H$, whose rate is larger at the center of the reactor owing to the maximum of the electron density profile there. Figs. 3 and 4 show the profiles of the steady-state concentration of silylene, SiH_2, and silyl, SiH_3, respectively. The

Table 2
Reaction rate constants

Reaction	Rate constant	Units
$e^- + SiH_4 \rightarrow SiH_2 + 2H$	$k_1 = 1.870 \times 10^{-11}$	$s^{-1}\ cm^3$
$e^- + SiH_4 \rightarrow SiH_3 + H$	$k_2 = 1.590 \times 10^{-10}$	$s^{-1}\ cm^3$
$H + SiH_4 \rightarrow SiH_3 + H_2$	$k_3 = 1.325 \times 10^{12}$	$s^{-1}\ mol^{-1}\ cm^3$
$SiH_3 + SiH_3 \rightarrow SiH_4 + SiH_2$	$k_4 = 9.033 \times 10^{13}$	$s^{-1}\ mol^{-1}\ cm^3$
$SiH_4 + SiH_2 \rightarrow Si_2H_6$	$k_5 = 2.830 \times 10^{13}$	$s^{-1}\ mol^{-1}\ cm^3$

Table 3
Physico-chemical properties of plasma species

Properties	SiH_4	SiH_2	SiH_3	H	Units
D_i	285.05	321.86	319.16	2107.75	$cm^2\ s^{-1}$
c_i^0/c_t	1.0	0.0	0.0	0.0	
$c_{w,i}/c_i$	1.0	0.0	0.0	0.0	
γ_i	0.0	0.0	0.6	0.0	
s_i	0.0	1.0	0.4	0.0	

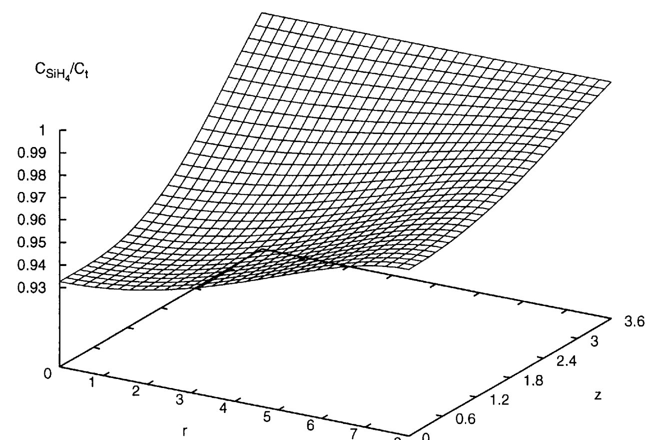

Fig. 2. Open-loop steady-state concentration profile of SiH_4 as a function of radius and height.

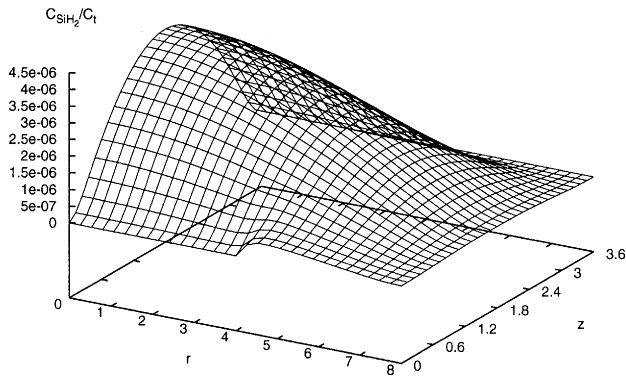

Fig. 3. Open-loop steady-state concentration profile of SiH_2 as a function of radius and height.

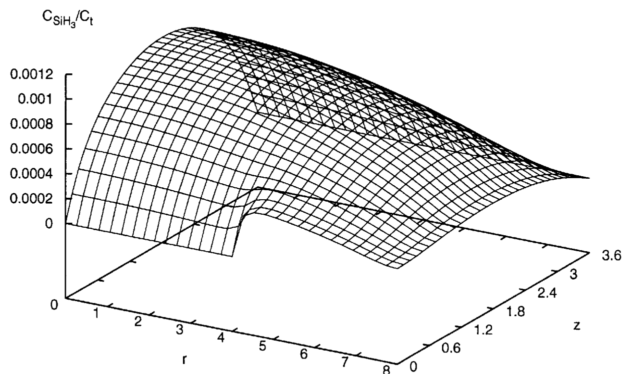

Fig. 4. Open-loop steady-state concentration profile of SiH_3 as a function of radius and height.

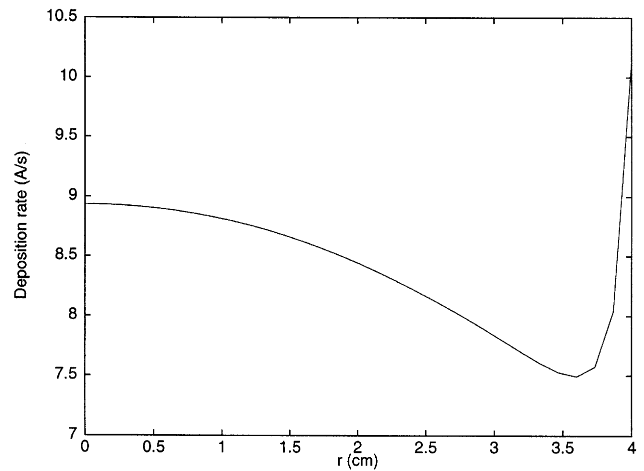

Fig. 5. Open-loop steady-state deposition rate of a − Si as a function of wafer radius.

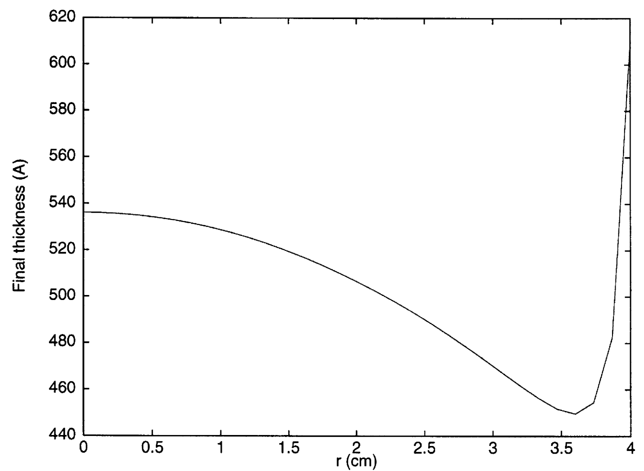

Fig. 6. Open-loop final thickness of a − Si film as a function of radius.

concentration of SiH_3 is much higher than the concentration of SiH_2 due to the higher reactivity of SiH_2 in the bulk of the plasma (see also Gallagher (1988) and Doyle et al. (1990) for similar observations). The low concentration of SiH_2 decreases the role of the reactions of this species that lead to a − Si deposition, and suggests that amorphous silicon is mainly produced by SiH_3 consumption. As expected, the maximum steady-state concentration for both SiH_2 and SiH_3 is located at the center of the reactor due to the maximum of the electron density in this location.

The nonuniform concentration of SiH_3 on the wafer surface, together with the fact that the deposition rate is mainly determined by the deposition reaction of SiH_3, create a nonuniform deposition rate profile for amorphous silicon along the radius of the wafer (Fig. 5). This results in a radially nonuniform final film thickness profile which is shown in Fig. 6. A measure of the spatial nonuniformity, say M_N, can be defined as $M_N = (H_{\max} - H_{\min})/H_{\min}$, where H_{max}, H_{min} are the maximum and minimum height of the film for $0 \text{ cm} \leqslant r \leqslant 3.6 \text{ cm}$. The large film thickness nonuniformity appeared for $3.6 \text{ cm} \leqslant r \leqslant 4.0 \text{ cm}$ is due to the large gradient on the concentration of SiH_2 and SiH_3 at the wafer edge (Fig. 3; this is a result of the fact that SiH_2 and SiH_3 do not react with the walls of the reactor), and it will not be accounted for in M_N because it occurs in a region which is not utilized for the placement of an integrated circuit. Using the values for H_{max}, H_{min} from Fig. 6, the nonuniformity measure for the open-loop process is computed to be $M_N = 19.2\%$. This is a very large value, according to any industrial standard, which suggests the implementation of a feedback control system on the PECVD process to reduce radial film thickness nonuniformity.

4. Controller design — closed-loop simulations

We now design and implement a feedback control system on the PECVD process in order to reduce the radial nonuniformity of the deposition rate and final film thickness. The proposed control system utilizes point

measurements of the deposition rate at several locations across the radius of the wafer to manipulate the inlet concentration of silane in the showerhead and achieve spatially uniform deposition of the 500 Å amorphous silicon thin film. The concentration of silane at the showerhead was chosen as the manipulated variable because of its strong effect on the deposition rate (this was verified with several open-loop simulation runs for different inlet silane concentrations; the effect of the inlet flow rate on the deposition rate was also examined and found to be negligible). Furthermore, the choice of the inlet silane concentration as manipulated variable was motivated by the realization that the suppression of radial deposition rate nonuniformity requires the use of a manipulated variable that is distributed across the radius of the wafer. We note that in practice, the inlet silane concentration is manipulated by adjusting the composition of an inert gas such as H_2 or He (Luft and Tsuo, 1993) in the feed to the showerhead (the use of such a diluent does not affect the velocity profile inside the reactor, i.e., v_w remains constant). Owing to the mildly nonlinear nature of the process model of Eq. (11) (it only includes bilinear nonlinearities since the assumption of isothermal operation allows considering the reaction rate parameters independent of temperature), a linear proportional integral (PI) controller with the following state-space description:

$$\dot{\xi} = y_{sp} - y, \qquad \xi(0) = 0,$$
$$u = K(y_{sp} - y) + \frac{1}{\tau}\xi \tag{18}$$

was initially used to manipulate the inlet concentration of silane throughout the showerhead to achieve offsetless set-point tracking. In the controller of Eq. (18), ξ is the controller state variable, y_{sp} denotes the set-point value of the deposition rate, y denotes the *on-line measurement* of the deposition rate, K is the proportional controller gain and τ is the integral time constant. The manipulated input u was defined as $u = c_{w,1}/c_t$, where $c_{w,1}$ represents the concentration of silane at the showerhead, and the controlled output was defined as

$$y(t) = \frac{1}{\rho_{si}} \int_0^{r_w} \left[\sum_{i=1}^{4} s_i D_i \frac{\partial c_i}{\partial z}(t, r, 0) \right] \mathrm{d}r$$

where r_w is the radius of the wafer, and was computed by using 30 measurements of the deposition rate across the wafer. In practice, a variety of on-line measurement techniques can be employed to determine the thickness of the deposited film in situ (and thus, the deposition rate), such as ellipsometry (Luft and Tsuo, 1993) and transient photoconductivity (Neitsert et al., 1995). y_{sp} was set equal to 6.9 Å/s which means that the time required for the growth of a 500 Å thin film is approximately 73 s (the corresponding time for the open-loop process is 60 s). Fig. 7 shows the closed-loop final film thickness as a function of wafer radius, while Fig. 8 shows the corresponding manipulated input profile (note that $u = 0.0$ means that no silane enters the reactor, while $u = 1.0$ means that the feed consists of pure silane). The controller decreases the radial nonuniformity of the final thickness to $M_N = 10.2\%$ (note that in the open-loop system the nonuniformity is $M_N = 19.2\%$). Even though the use of a single PI controller reduces the film thickness nonuniformity compared to the one of the open-loop process, the reduction obtained is not significant enough, thereby motivating the design of a new feedback control system.

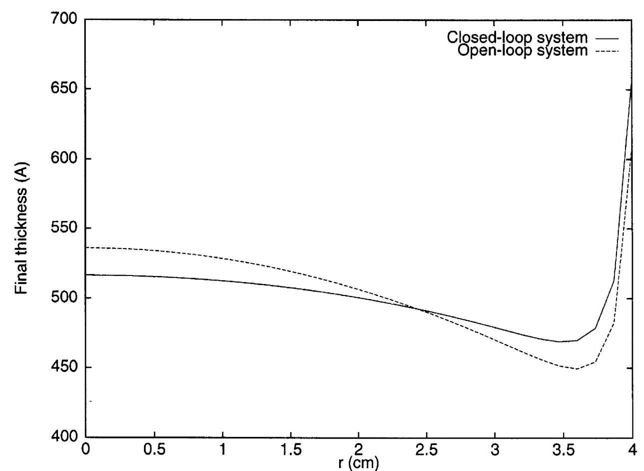

Fig. 7. Controlled final thickness of a − Si film across the radius of the wafer (single PI controller).

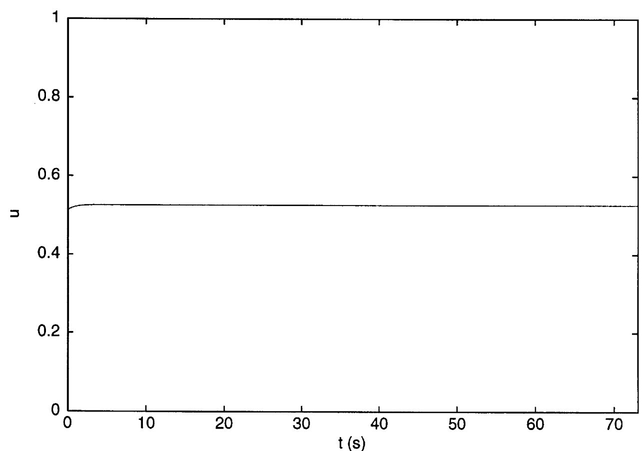

Fig. 8. Manipulated input profile for a single PI controller.

To further reduce the film thickness nonuniformity, we divide the showerhead area into three concentric regions (Fig. 9) and use three PI controllers to adjust the inlet silane concentration in each one of these regions. We note that no controller was used in the showerhead region which is outside of the wafer. The idea of dividing the showerhead region into three concentric subregions

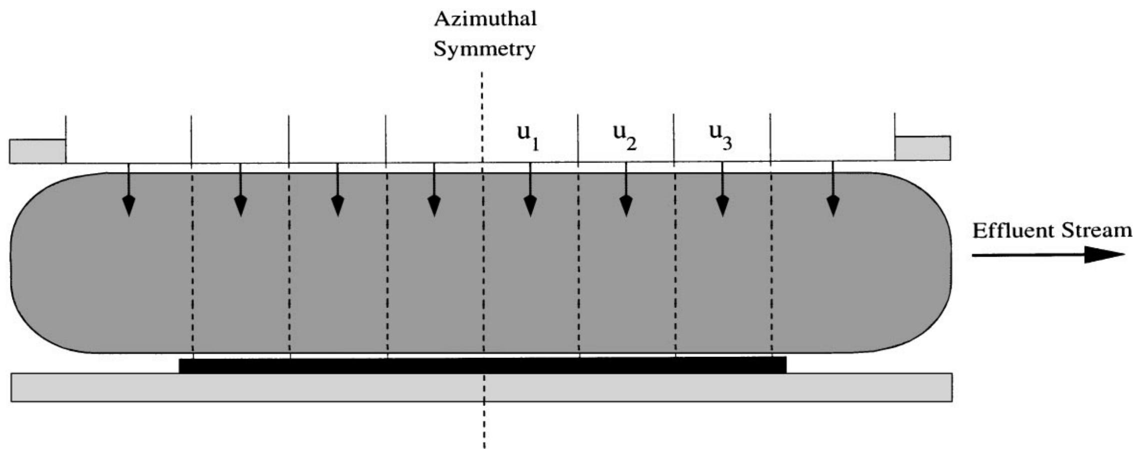

Fig. 9. Control configuration for PECVD reactor.

is based on the realization that the effective control of a variable that is distributed in space (as is the case with the deposition rate in this problem) should be achieved by independently controlled manipulated inputs that are also distributed in space. The state-space representation of the feedback control system takes then the form:

$$\dot{\xi}_\kappa = y_{sp,\kappa} - y_\kappa, \quad \xi_\kappa(0) = 0, \quad \kappa = 1, 2, 3,$$
$$u_\kappa = K_\kappa(y_{sp,\kappa} - y_\kappa) + \frac{1}{\tau_\kappa}\xi_\kappa, \tag{19}$$

where the κth controlled output is defined as

$$y_\kappa(t) = \frac{1}{\rho_{Si}} \int_{r_{s,n}}^{r_{f,n}} \left[\sum_{i=1}^{4} s_i D_i \frac{\partial c_i}{\partial z}(t,r,0) \right] \mathrm{d}r,$$

where $r_{s,\kappa}$, $r_{f,\kappa}$ are the internal and external radii of the region where the κth control action is applied, and $y_{sp,\kappa}$ is the set-point for the κth region. Table 4 below provides the parameters and set-point values for the three PI controllers, and the radii of the regions where they are applied.

Fig. 10 shows the closed-loop final thickness in the case of using three PI controllers, while Fig. 11 displays the corresponding manipulated input profiles. It is clear that the use of three spatially distributed PI controllers has substantially reduced the film thickness nonuniformity; the nonuniformity measure for the profile of Fig. 10 is $M_N = 3.8\%$ which is much less than 19.2% (uncontrolled process) and 10.2% (single PI controller). We also tested the robustness properties of the proposed PI control system in the presence of modeling errors. Specifically, the value of n_{eo} was assumed to vary, in a sinusoidal fashion, 20% around the nominal value of Table 1 with a period of 4.0 s, for the first 20 s of operation of the process. Fig. 12 displays the final film thickness profile for this simulation run. The thickness nonuniformity measure is again $M_N = 3.8\%$, thereby indicating that the proposed control system possesses excellent robustness properties with respect to significant modeling errors.

Table 4
Parameters for the 3 PI controllers

κ	K_κ	τ_κ (s)	$r_{s,\kappa}$ (cm)	$r_{f,\kappa}$ (cm)	$y_{sp,\kappa}$ (A/s)
1	0.5	1.25	0.0	2.0	6.9
2	0.5	1.25	2.0	3.0	6.9
3	0.5	1.25	3.0	4.0	6.9

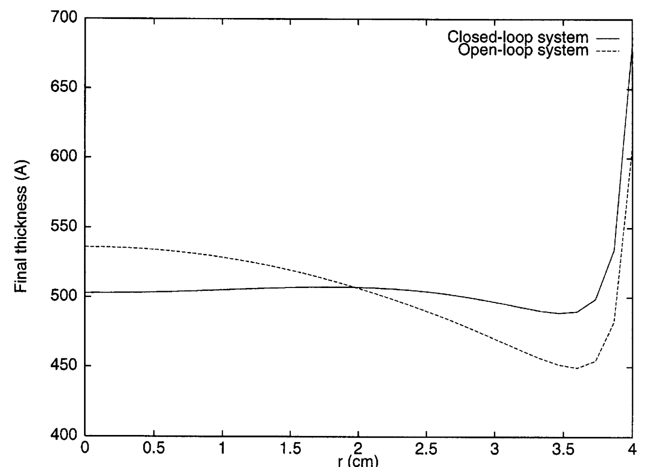

Fig. 10. Controlled final thickness of a − Si film across the radius of the wafer (three PI controllers).

Remark 1. From the above closed-loop system simulation results, it is evident that the division of the showerhead region into three concentric subregions is the main reason for the significant reduction in film thickness nonuniformity. To further establish this observation, we carried out several simulation runs using more than three concentric regions and PI controllers, and found that further reduction on the film thickness nonuniformity was achieved (i.e. the resulting M_N was less than 3.8%). Even though the use of more than three concentric subregions is not particularly meaningful for the deposition

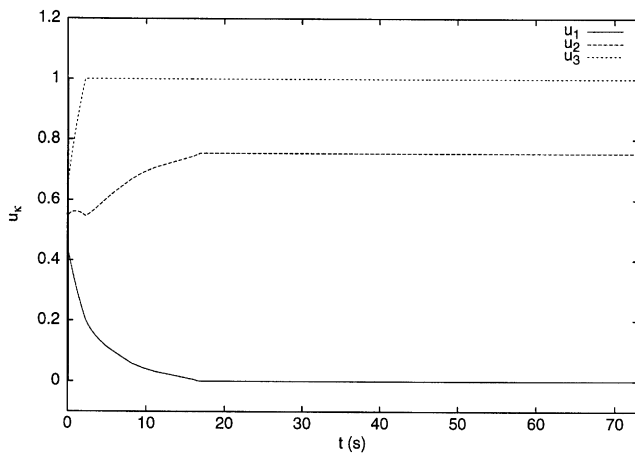

Fig. 11. Manipulated input profiles for the three PI controllers.

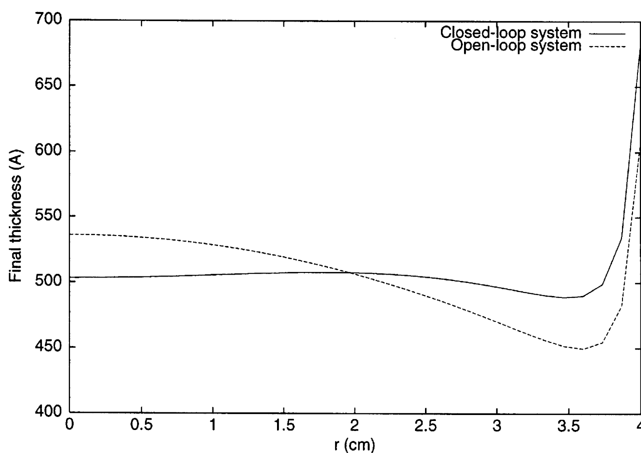

Fig. 12. Controlled final thickness of a – Si film across the radius of the wafer in the presence of model uncertainty (three PI controllers).

problem studied in this paper (since $M_N = 3.8\%$ is already very small), it should be definitely examined in the case of film deposition on larger wafers (e.g., 4.0 in wafer instead of 8.0 cm one), where the open-loop film thickness nonuniformity is going to be considerably higher than 19.2%.

5. Conclusions

In this work, we studied the modeling and control of a single-wafer parallel electrode PECVD process with showerhead arrangement used to deposit a 500 Å amorphous silicon thinfilm on an 8 cm wafer. Initially, a two-dimensional unsteady-state model was developed for the process that accounts for diffusive and convective mass transfer, bulk and deposition reactions, and nonuniform fluid flow and plasma electron density profiles. The model was solved using finite-difference techniques and the radial film thickness nonuniformity was found to be 19.2%. Then, a feedback control system was designed and implemented on the process to reduce the film thickness nonuniformity. The control system consists of three spatially distributed proportional integral controllers that use measurements of the deposition rate at several locations across the wafer, to manipulate the inlet concentration of silane in the showerhead and achieve a uniform deposition rate across the wafer. The implementation of the proposed control system was shown to reduce the film thickness nonuniformity to 3.8%. The proposed control system was also found to be robust with respect to modeling errors. We finally note that even though this study focused on the deposition of an amorphous silicon thin film, the developed numerical model and control strategy can be readily applied to other plasma-assisted processes (e.g. plasma etching) and chemistries.

Acknowledgements

Financial support from a National Science Foundation CAREER award, CTS-9733509, is gratefully acknowledged.

Notation

c_1	concentration of silane SiH_4
c_2	concentration of silylene radical SiH_2
c_3	concentration of silyl radical SiH_3
c_4	concentration of atomic hydrogen H
c_t	total concentration of species in chamber
c_i^0	initial concentration of ith species
$c_{w,i}$	concentration of ith species at the showerhead
D_1	self-diffusion coefficient of SiH_4
D_2	diffusion coefficient of SiH_2 in SiH_4
D_3	diffusion coefficient of SiH_3 in SiH_4
D_4	diffusion coefficient of H in SiH_4
H_{max}	maximum height of deposited film
H_{min}	minimum height of deposited film
k_i	reaction rate constant of ith reaction
K_κ	proportional gain of the κth controller
L	height of the chamber
M_N	spatial nonuniformity
n_e	electron density
n_{eo}	maximum electron density
N_h	number of openings on the showerhead
P	pressure inside the chamber
Q	volumetric flow rate of influent stream
r	radial coordinate
r_h	radius of the openings of the showerhead
$r_{f,\kappa}$	maximum radius of the region of application of the κth controller
$r_{x,i}$	reaction rate of ith reaction

$r_{s,\kappa}$ minimum radius of the region of application of the κth controller
r_t radius of the chamber
r_w radius of the wafer
Re_w wall Reynolds number
R_{dep} deposition rate
s_i sticking coefficient of ith species on the wafer surface
t temporal coordinate
T temperature inside the chamber
u_κ control action of the κth controller
v_r radial velocity
v_w axial velocity at the showerhead
v_z axial velocity
y_κ controlled output of the κth controller
$y_{sp,\kappa}$ set point of the κth controller
z axial coordinate

Greek letters

γ_i recombination coefficient of ith species
ξ_κ state of the κth controller
μ viscosity of plasma
ν kinematic viscosity of plasma
ρ density of plasma
ρ_{Si} density of amorphous silicon
τ_κ integral gain of the κth controller
ψ spatial parameter

Math symbols

J_0 zero order Bessel function
$\int_a^b f\,dz$ integration of function f with respect to variable z over the interval $[a, b]$
$\partial f/\partial z$ partial derivative of function f with respect to variable z

References

Austin, E. R., & Lampe, F. W. (1976). Hydrogen-atom initiated decomposition of monosilane. *J. Phys. Chem., 80,* 2811–2817.

Belenguer, P., & Boeuf, J. P. (1990). Transition between different regimes of RF glow discharges. *Phys. Rev. A*, *41*, 4447–4459.

Bohm, C. and Perrin, J. (1991). Spatially resolved optical emission and electrical properties of SiH_4 RF discharges at 13.56 MHz in a symmetric parallel-plate configuration. *J. Phys. D*: *Appl. Phys.*, *24*, 865–881.

Caquineau, H., & Despax, B. (1997). Influence of the reactor design in the case of silicon nitride PECVD. *Chem. Engng. Sci.*, *52*, 2901–2914.

Doughty, D. A., Doyle, J. R., Lin, G. H., & Gallagher, A. (1990). Surface reaction probability of film-producing radicalsin silane glow discharges. *J. Appl. Phys.*, *67*, 6220–6228.

Doyle, J. R., Doughty, D. A., & Gallagher, A. (1990). Silane dissociation products in deposition discharges. *J. Appl. Phys.*, *68*, 4375–4384.

Economou, D. J., Park, S., & Williams, G. D. (1989). Uniformity of etching in parallel plate plasma reactors. *J. Electrochem. Soc.*, *136*, 188–198.

Gallagher, A. (1988). Neutral radical deposition from silane discharges. *J. Appl. Phys.*, *63*, 2406–2413.

Hamby, E. S., Kabamba, P. T., & Meerkov, S. M. (1994). A system-theoretic approach to modeling and analysis of deposition rate uniformity in PECVD. *Proc.* 33*rd IEEE Conf. on Decision and Control*, Lake BuenaVista, FL, pp. 86–90.

Hirschfelder, J. O., Curtiss, C. F., & Bird, R. B. (1954). *Molecular theory of gases and liquids*. New York: Wiley.

Kushner, M. J. (1988). A model for the discharge kinetics and plasma chemistry during plasma enhanced chemical vapor deposition of amorphous silicon. *J. Appl. Phys.*, *63*, 2532–2551.

Layeillon, L., Dollet, A., Couderc, J. P., & Despax, B. (1994a). Analysis and modeling of plasma enhanced CVD reactors. part I: Two-dimensional treatment of $a-$ Si: H deposition. *Plasma Sources Sci. Technol.*, *3*, 61–71.

Layeillon, L., Dollet, A., Couderc, J. P., & Despax, B. (1994b). Analysis and modeling of plasma enhanced CVD reactors. part II: Model improvement and systematic use. *Plasma Sources Sci. Technol.*, *3*, 72–79.

Layeillon, L., Dollet, A., & Despax, B. (1995). Plasmaenhanced deposition of $a-Si$: Comparison of two reactor arrangements. *Chem. Engng J.*, *58*, 1–5.

Luft, W., & Tsuo, Y. S. (1993). *Hydrogenated amorphous silicon alloy deposition processes*. USA: Marcel Dekker.

McLaughlin, K. J., Butler, S. W., Edgar, T. F., & Trachtenberg, I. (1991a). Development of techniques for real-time monitoring and control in plasma etching i. response surface modeling of CF_4/O_2 and CF_4/H_2 etching of silicon and silicon dioxide. *J. Electrochem. Soc.*, *138*, 789–799.

McLaughlin, K. J., Butler, S. W., Edgar, T. F., & Trachtenberg, I. (1991b). Development of techniques for real-time monitoring and control in plasma etching i. multivariable control system analysis of manipulated, measured and performance variables. *J. Electrochem. Soc.*, *138*, 2727–2735.

Mozumder, P. K., Saxena, S., & Collins, D. J. (1994). A monitor wafer based controller for semiconductor processes. *IEEE Trans. Semicond. Mfg.*, *7*, 400–411.

Neitzert, H. C., Hirsch, W., Kunst, M., & Nell, M. E. A. (1995). *In situ* thickness control during plasma deposition of hydrogenated amorphous silicon films by time-resolved microwave conductivity measurements. *Appl. Opt.*, *34*, 676–680.

Park, S., & Economou, D. J. (1990). Numerical simulation of a single-wafer isothermal plasma etching reactor. *J. Electrochem. Soc.*, *137*, 2624–2634.

Park, S., & Economou, D. J. (1991). A mathematical model for etching of silicon using CF_4 in a radial flow plasma reactor. *J. Electrochem. Soc.*, *138*, 1499–1508.

Perrin, J., & Broekhuizen, T. (1987). Surface reaction and recombination of the SiH_3 radical on hydrogenated amorphous silicon. *Appl. Phys. Lett.*, *50*, 433–435.

Perrin, J., Takeda, Y., Hirano, N., Takeuchi, Y., & Matsuda, A. (1989). Sticking and recombination of the SiH_3 radical on the hydrogenated amorphous silicon: The catalytic effect of diborane. *Surf. Sci.*, *210*, 114–128.

Reid, R. C., Prausnitz, J. M., & Poling, B. E. (1987). *The properties of gases and liquids* (4th ed.) USA: McGraw-Hill.